



ANALYSIS OF EXHAUST MANIFOLD OF 4-CYLINDER SI ENGINE USING CFD

¹Abhishek Srivastava, ²Dr. Shailendra Sinha

¹M.tech (Mechanical Engineering),

²Professor, Department of Mechanical Engineering

Institute of Engineering and Technology, Lucknow

ABSTRACT

An exhaust manifold collects the exhaust gases from multiple cylinders into one single pipe. The exhaust manifold of engine is mounted on cylinder head and used for removing exhaust gases from the engine cylinder effectively. Exhaust pipes for each cylinder are commonly connected to common header called exhaust manifold. The purpose of present work is to investigate the best geometry and the position of tail pipe on the exhaust header. The exhaust manifold of an engine can have problems of crack and extensive plastic deformations, and the finite volume method is being applied to predict thermal stress and deformations in manifold area. The present study is carried out to investigate the pressure drop and thermal deformations of an exhaust manifold using CFD.

KEYWORDS- IC Engine, Exhaust manifold, Finite volume method, CFD analysis, Pressure drop, thermal deformations.

1. INTRODUCTION

The Exhaust Manifold is the key component in the exhaust system on a vehicle. It is responsible for collecting the exhaust gas from the engine's cylinder heads and sending it down to the exhaust pipe. At the same time, it prevents any toxic exhaust fumes from leaking into the passenger area of the vehicle. Exhaust manifolds come in two main design styles, commonly referred to as four-into-one and four-into-two exhaust manifolds. Most exhaust manifolds are made from cast iron, but aftermarket versions are often made from welded tubular steel.

Exhaust manifolds are a necessary component of the exhaust system. Their design is optimized to ensure exhaust gases flow efficiently from the engine combustion chamber without creating any back pressure. A properly functioning exhaust manifold is important to prevent uneven power and engine vibrations. Exhaust manifolds are made either from cast iron or one of a few types of steel. The majority of exhaust manifolds are made from cast iron, as it is relatively inexpensive and lasts a long time. The drawbacks to cast iron manifolds are that they are quite heavy and tend to get brittle with age and exposure to the heat cycles of an engine.

Tubular steel exhaust manifolds are known for having better exhaust flow and are, therefore, found on many performance vehicles. Stainless steel exhaust manifolds are the most expensive, but are rust-resistant and extremely long lasting. Less expensive aluminized steel manifold offer many of the benefits of stainless ones, but will rust if the outer layer is scratched. Exposure to the normal heat cycles of an engine can cause cracks in an exhaust manifold. As the vehicle continues to age, the cracks turn into holes. Once this happens, the vehicle engine sounds extremely loud and there is a likely chance that toxic fumes are entering the cabin of the vehicle. The gaskets on the exhaust manifold are equally important, and their failure has the same results. Other exhaust manifold components that are subject to failure include the exhaust system hangers, which are designed to hold up the entire system. These can break off, leaving the whole weight of the exhaust system to be carried by the manifold, and eventually causing it to fail.

2. METHODOLOGY

2.1 MODEL DESCRIPTION

In the present work, an exhaust system of 4-Cylinder SI engine of existing model having runner diameter 37.5mm, having varying bent radius 46.875, 56.25, 70.3125, 89.0625 and 112.5mm is taken for consideration and overall length of pipe is 168.8mm is considered. The inner diameter of pipe is taken as 37.5mm and outer diameter is taken as 41.07mm. In existing model the position of the tail pipe is at one end of the header. This model has been compared with the exhaust system having the position of the tail pipe at the centre of the header which is the modified model of an exhaust system. The diameter of the runner of the modified model is 37.5mm at varying bent radius are in the order of 46.875, 56.25, 70.3125, 89.0625 and 112.5mm. Overall length of the pipe remain at 168.8mm. Fig 1 and Fig 2 shows the schematic diagram of exhaust system of existing and modified type model.

Other parameters like density, specific enthalpy, specific entropy, Specific heat at constant temperature and dynamic viscosity are later used for the calculation of pressure drop. Both existing and modified model has header length of 335mm. The diameter of headers for both the model are 50mm respectively. Exhaust gas temperature at 773K and mass flow rate of 0.0684kg/sec is taken for the consideration of fluid flow at the inlet of exhaust pipes for both the type of model.

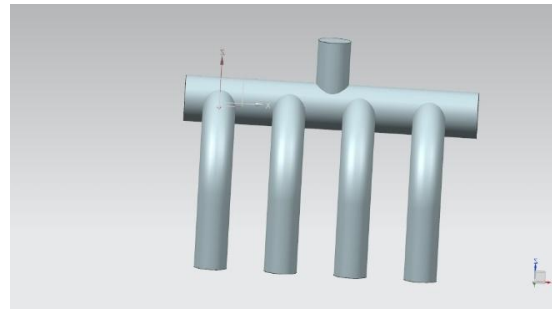
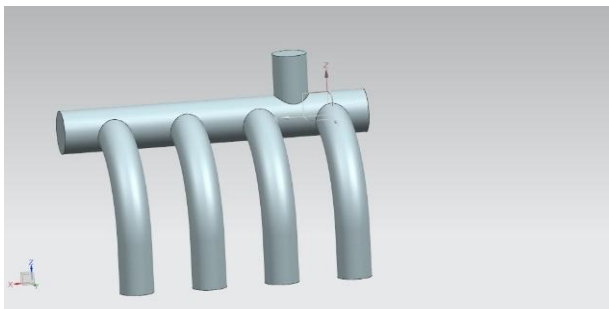


Fig. 1: Existing Model Fig. 2: Modified Model

Both the models considered for this work were prepared using **UNIGRAPHICS NX** software. These models were imported into **ANSYS CFD V17.0**. The fluid body was subsequently generated from existing model and modified model using design modular in ANSYS and subsequently meshed as shown in figure.

2.2 FLUID PROPERTIES

Exhaust gas will be considered as an incompressible fluid operating between 400-600⁰ C. The material properties under these conditions are:-

Table 1: FLUID PROPERTIES^[REF: 16]

Fluid	Exhaust gas
Density	0.435 kg/m ³
Specific enthalpy	822.5 KJ/kg
Specific entropy	7.888 KJ/Kg-k
Specific heat at constant pressure(C _p)	1.099 KJ/Kg-k
Viscosity	3.7 * 10 ⁻⁵ Pa-s
Thermal conductivity	0.0577 w/m-k



2.3 MATHEMATICAL FORMULATION

• **Governing Equations:-** The flow is assumed to be two dimensional, steady, incompressible and constant laminar viscosities. Therefore, the mean flow is assumed to satisfy the incompressible Navier- Stokes equations with an eddy viscosity. A set of the differential equations which are commonly used to depict the flow under prescribed conditions can be presented in a general form.

$$\frac{\partial y}{\partial x}(\rho u \phi) + \frac{\partial y}{\partial x}(\rho v \phi) = \frac{\partial y}{\partial x} \left(\Gamma \phi \frac{\partial y}{\partial x} \right) + \frac{\partial}{\partial y} \left(\Gamma \phi \frac{\partial y}{\partial x} \right) + S_{x,y} \dots \dots \dots (1)$$

Equation (1) is called the general transport equation. The argument ϕ identifies the dependent variable, Γ is the diffusion coefficient for variable ϕ . The two terms on the left-hand side are the convective terms; the first two terms on the right-hand side are the diffusive term, and the last term is the source term. The source term includes both the source of ϕ and any other terms that cannot find place in any of the convection or diffusion terms. The governing differential equations in engineering problems are generally derived in Cartesian (i.e. rectangular) coordinate systems. Finite difference methods for solving differential equations require that continuous physical space is to be discretized into a uniform orthogonal computational space. Difficulties associated with the use of Cartesian coordinate system motivate the introduction of a transformation from physical (x, y) space to a generalized curvilinear coordinate (ξ, η) space. The final complete transformed form of the conservative general transport equation for property ϕ can be written, as follows:

$$\frac{\partial}{\partial \xi} (\rho G_1 \phi) + \frac{\partial}{\partial \eta} (\rho G_2 \phi) = \frac{\partial}{\partial \xi} (J \Gamma \phi \phi_{\xi} a_1) + \frac{\partial}{\partial \eta} (J \Gamma \phi \phi_{\eta} a_2) + S_{total} \dots \dots \dots (2)$$

Where:
 S_{total} : represents the total source term

$$S_{total} = JS_{x,y} + S_{\xi,\eta} \dots \dots \dots (3)$$

Discretisation method

The finite-volume method of will be used for the discretization of the conservative form of the governing equations. The calculations domain is divided into a number of non-overlapping control volumes surrounding each grid point Then, the governing equations can be integrated over discrete control volume in the computational space. Final discretized algebraic equation for property ϕ is given by the following:

$$A_P \phi_P = \sum_{nb} A_{nb} \phi_{nb} + S_{total} \nabla V \dots \dots \dots (4)$$

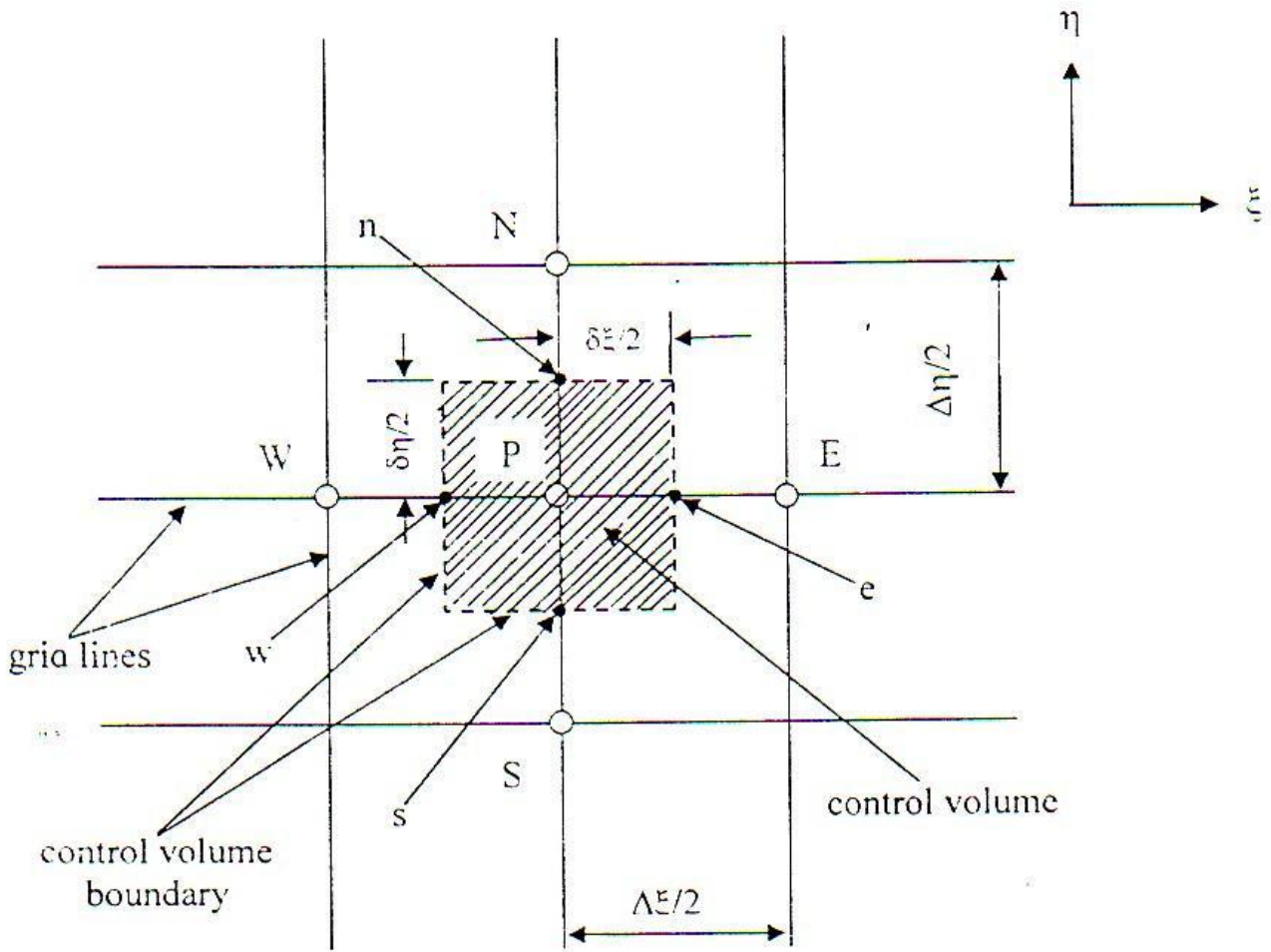


Fig 3: Control Volume arrangement for general variable

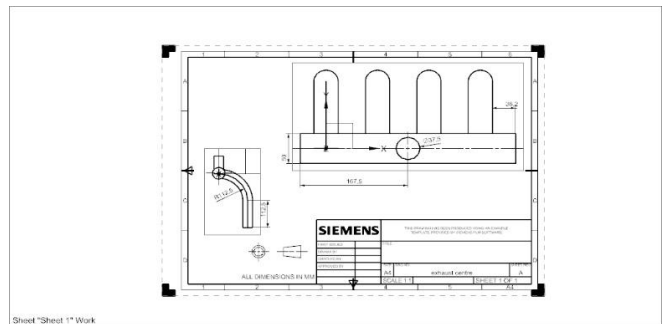
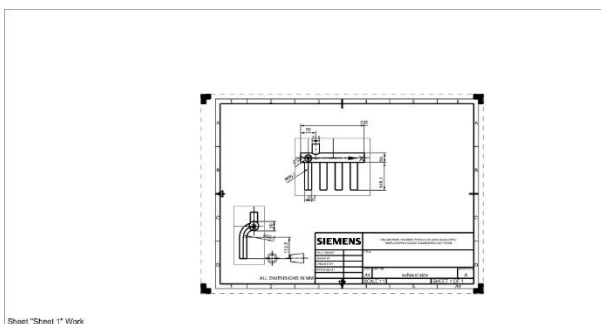


Fig.4 Two dimensional manifold geometry for existing and modified model

- Inlet boundary condition:** The distribution of all flow variables are specified at inlet boundaries (the line $I=1$ or $i=2$ for u_x velocity). An approximation for the inlet distribution for k and ϵ as given below:



$$K = \frac{2}{3}(u_{\xi in} T_i)^2 \dots\dots\dots(5)$$

$$\epsilon = C\mu^{3/4} \frac{K^{3/2}}{l} \dots\dots\dots (6)$$

$$l = 0.07 L \dots\dots\dots(7)$$

where:

L : is equivalent hydraulic diameter,

$C\mu$: is a universal constant, 0.09,

l : is the length scale of turbulence and

T_i : turbulence intensity.

- **Outlet Boundary Conditions:** The gradient of all variables at the outlet are specified equal to zero.
- **Wall Boundary Conditions:** The optimum near wall relationships for the standard k-ε model from extensive computing trials are implemented as follows.
- **Momentum equation tangential to wall**

Wall shear stress:

$$\tau_w = \rho C\mu^{1/4} K_p^{1/2} u_p / u^+ \dots\dots\dots(8)$$

Wall force:

$$F_s = -\tau_w A_{cell} = \rho C\mu^{1/4} K_p^{1/2} u_p / u^+ A_{cell} \dots\dots\dots(9)$$

- **Momentum equation normal to wall**

Normal velocity= 0

Turbulent kinetic energy equation

$$\text{Net-k source per unit volume} = (\tau_w u_p - \rho C\mu^{1/4} K_p^{3/2} u^+) \Delta V / \Delta y_p \dots\dots\dots(10)$$

- **Dissipation rate equation**

Set nodal value:

$$\epsilon = C\mu^{3/4} K_p^{3/2} / (K \Delta y_p) \dots\dots\dots(11)$$

where:

A_{cell} : is the wall area of control volume

These relationships should be used in conjunction with universal velocity (u^+) for near wall turbulent flows:

$$\mu^+ = \frac{1}{\kappa} \ln(E y^+) \dots\dots\dots(12)$$

The governing equation was solved using upwind differences scheme, and the solution is repeated until convergences achieved.



2.3 BOUNDARY CONDITIONS FOR THE CALCULATION OF PRESSURE DROP USING CFD ANALYSIS IN EXHAUST MANIFOLD

A four stroke four cylinder gasoline engine has been considered for this case running at engine speed at 3000 rpm having mass flow rate of exhaust gas at 0.0684 kg/sec. The temperature of exhaust gases is 500⁰C(773 K). Atmospheric gauge pressure was set at 0 and pressure distribution was obtained over manifold area. Mass flow boundary conditions can be used in ANSYS Fluent to provide a prescribed mass flow rate or mass flux distribution at an inlet. As with a velocity inlet, specifying the mass flux permits the total pressure to vary in response to the interior solution. This is in contrast to the pressure inlet boundary condition, where the total pressure is fixed while the mass flux varies. However, unlike a velocity inlet, the mass flow inlet is equally applicable to incompressible and compressible flows. A mass flow inlet is often used when it is more important to match a prescribed mass flow rate than to match the total pressure of the inflow stream. An example is the case of a small cooling jet that is bled into the main flow at a fixed mass flow rate, while the velocity of the main flow is governed primarily by a (different) pressure inlet/outlet boundary condition pair. A mass flow inlet boundary condition can also be used as an outflow by specifying the flow direction away from the solution domain.

2.4 STRUCTURAL ANALYSIS OF EXHAUST MANIFOLD TO DETERMINE THERMAL DEFORMATIONS

Exhaust Manifolds are affected by thermal stresses and deformations due the temperature distribution, heat accumulation or dissipation and other related thermal quantities. Finite Volume Method(FVM) involves the solution of simultaneous and algebraic solution.

The attempt has been made to find the critical regions where the stress concentration is more due to temperature distribution on the model resulting to thermal stresses which in turn influence these mechanical stresses and lead to stress concentration at a particular region resulting in a fissure which slowly and steadily propagates to cause the failure of the complete component.

- Heat transfer analysis is performed to determine the temperature distribution.
- Importing the temperature results in structural analysis.
- Stress and thermal deformations have been calculated on fixing the inlet manifold pipes and outlet pipe is exposed to the environment in cfd analysis.

In this analysis the material properties for temperature is 773K. The analysis was carried out in ANSYS 17.0 The material chosen for analysis is gray cast iron and following properties are shown below in a tabular form.

Table 2. MATERIAL PROPERTY(GRAY CAST IRON)^[REF:12]

Young's Modulus	110Gpa
Poisson's Ratio	0.28
Density	7200Kg/m ³
Thermal Expansion Coefficient	1.1*10 ⁻⁰⁵ / ⁰ C
Compressive Ultimate Strength	820 Mpa
Tensile Ultimate Strength	240 Mpa

3. RESULTS AND DISCUSSION

3.1 PRESSURE DISTRIBUTION IN EXHAUST EXISTING MODEL OVER BENT RADIUS

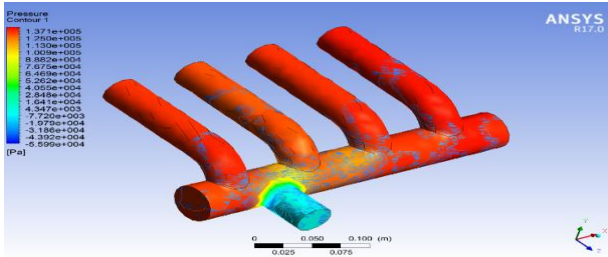


Fig.3.1: Pressure distribution for exhaust existing model at 46.875mm bent radius

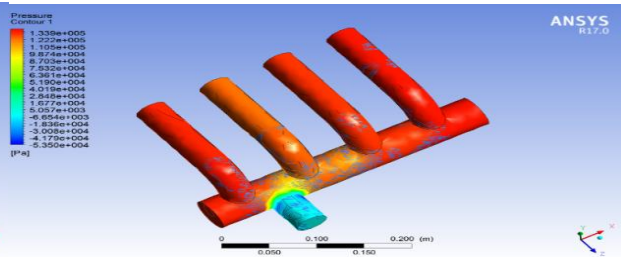


Fig 3.2: Pressure distribution for exhaust existing model at 56.25mm bent radius

Pressure distribution in existing type exhaust manifold is shown in fig 3.1 at 46.875mm and fig 3.2 at 56.25mm bent radius that varies inversely proportional to the pressure drop. The pressure drop is determined by observing the values of pressure at inlet and outlet and calculating the difference between

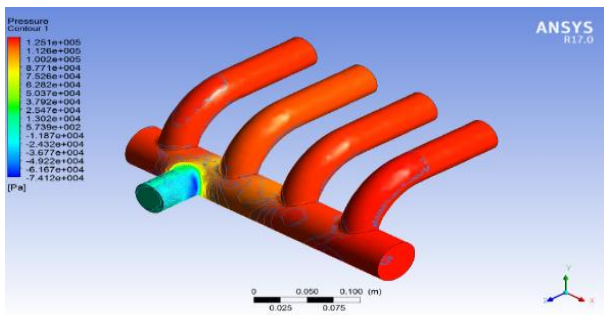


Fig. 3.3: Pressure distribution foreexhaust existing model at 70.3125mm bent radius

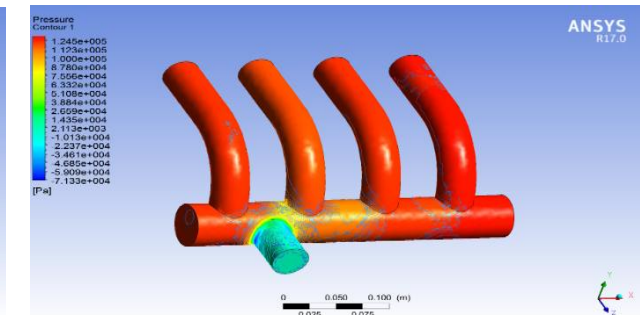


Fig.3.4: Pressure distribution foreexhaust existing model at 89.0625mm bent radius

Pressure distribution in existing type exhaust manifold is shown in fig 3.3 at 70.3125mm and fig 3.4 at 89.0625mm bent radius that varies inversely proportional to the pressure drop. The pressure drop is determined by observing the values of pressure at inlet and outlet and calculating the difference between them.

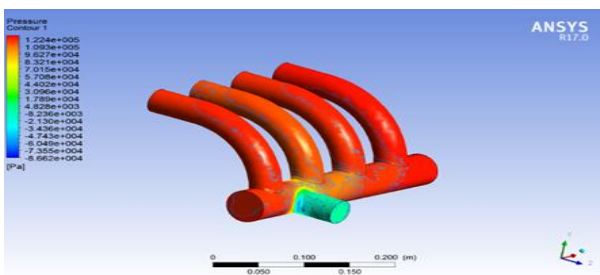


Fig.3.5: Pressure distribution foreexhaust existing model at 112.5mm bent radius

Pressure distribution in existing type exhaust manifold is shown in fig 3.5 at 112.5mm bent radius that varies inversely proportional to the pressure drop. The pressure drop is determined by observing the values of pressure at inlet and outlet and calculating the difference between them. The pressure drop is least for existing type exhaust manifold at 112.5mm bent radius.

3.2 PRESSURE DISTRIBUTION IN EXHAUST MODIFIED MODEL OVER BENT RADIUS

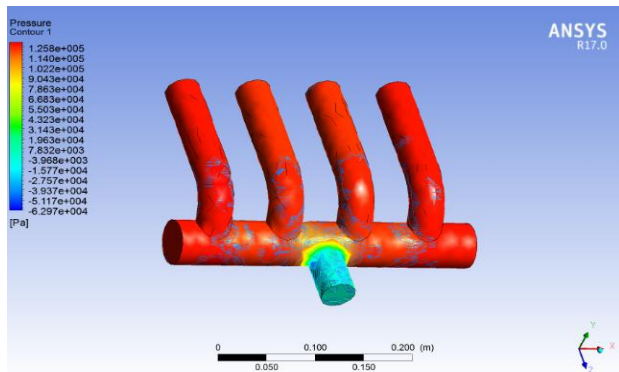


Fig.3.6: Pressure distribution for modified exhaust model at 46.875mm bent radius

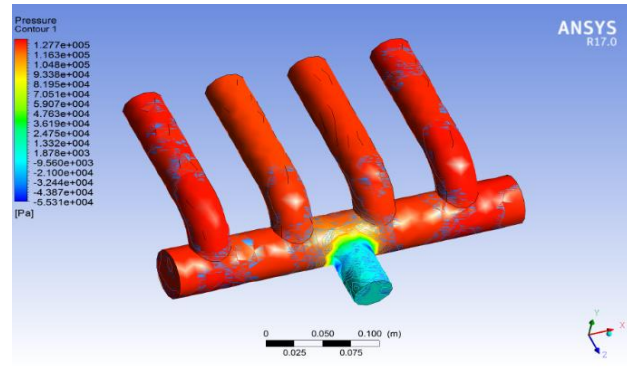


Fig.3.7: Pressure distribution for modified exhaust model at 56.25mm bent radius

Pressure distribution in modified type exhaust manifold is shown in fig 3.6 at 46.875mm and fig 3.7 at 56.25mm bent radius that varies inversely proportional to the pressure drop. The pressure drop is determined by observing the values of pressure at inlet and outlet and calculating the difference between them is less than existing type of exhaust manifold for same bent radius.

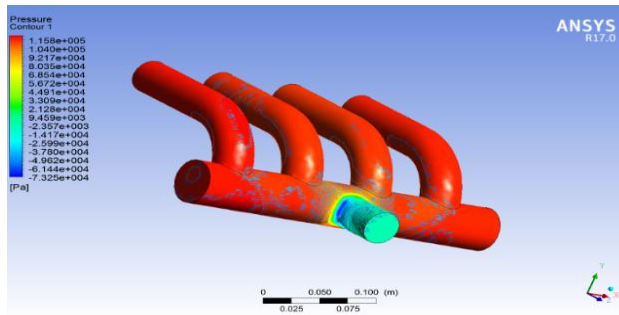


Fig.3.8: Pressure distribution for modified exhaust model at 70.3125mm bent radius

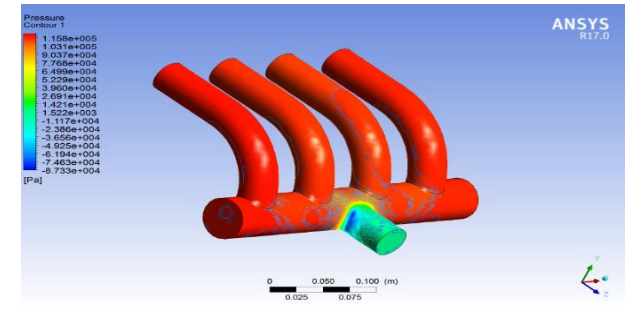


Fig.3.9: Pressure distribution for modified exhaust model at 89.0625mm bent radius

Pressure distribution in modified type exhaust manifold is shown in fig 3.8 at 70.3125mm and fig 3.9 at 86.0625mm bent radius that varies inversely proportional to the pressure drop. The pressure drop is determined by observing the values of pressure at inlet and outlet and calculating the difference between them is less than existing type of exhaust manifold for same bent radius.

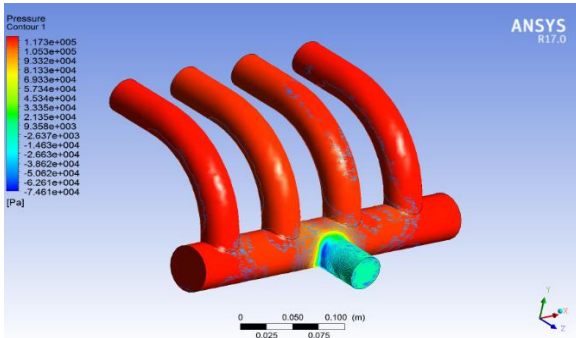


Fig.3.10: Pressure distribution for modified exhaust model at 112.5mm bent radius

Pressure distribution in modified type exhaust manifold is shown in fig 3.10 at 112.5mm bent radius that varies inversely proportional to the pressure drop. The pressure drop is determined by observing the values of pressure at inlet and outlet and calculating the difference between them. The pressure drop is least for modified type exhaust manifold at 112.5mm bent radius is less than existing type of exhaust manifold.

3.3 COMPARISON OF PRESSURE DROP FOR EXISTING AND MODIFIED MODEL

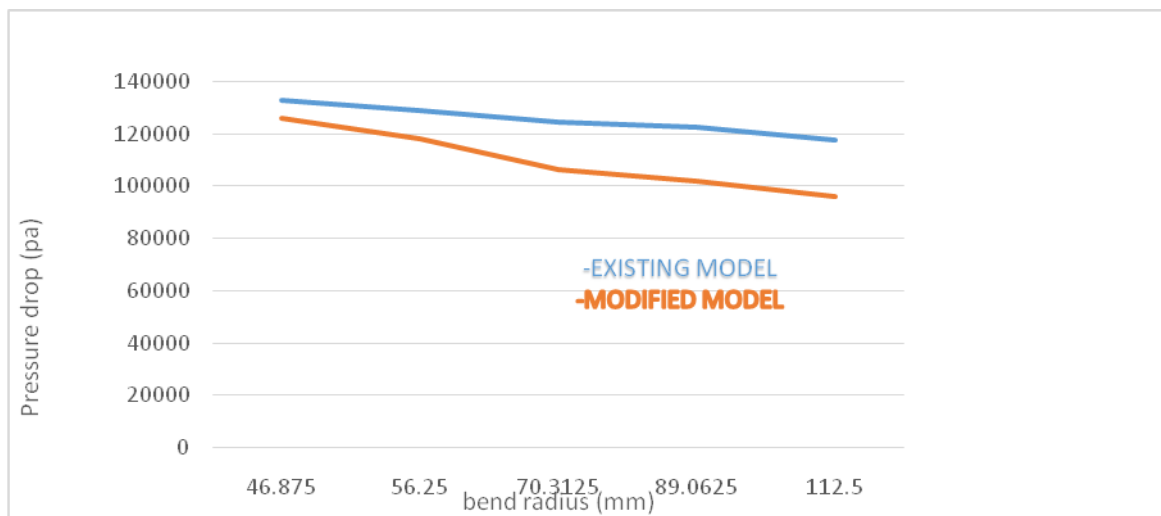


Fig 3.11: Comparison of pressure drop of an existing type as well as modified type exhaust manifold V/S bend radius

In the comparison of existing model and modified model the blue line shows the effective drop in pressure over bent radius for the existing model. When these values are compared with the modified model shown with orange line we found that pressure drop is more for each bent radius in the case of existing model and less for modified model. Comparing with the result of existing model the pressure drop is less for modified model and more for existing model, hence modifying the model is found to be appropriate. Variation in pressure drop over bent radius is also seen and found there is a reduced pressure drop for modified model when compared with that of existing model. So modifying the model is found to be appropriate.

3.4 THERMAL DEFORMATIONS IN EXISTING TYPE MANIFOLD

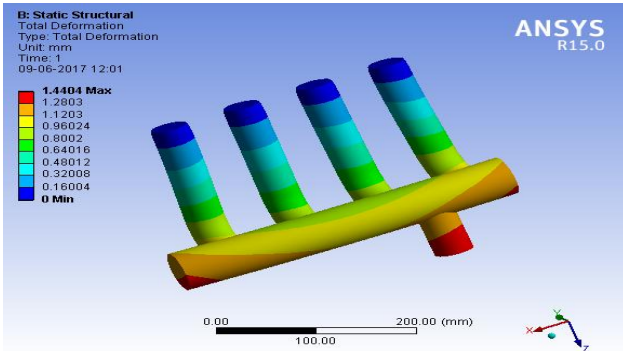


Fig 3.12: Thermal deformations for exhaust existing model at 46.875mm bent radius

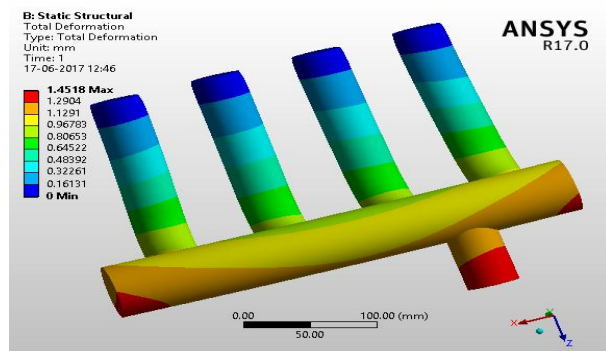


Fig 3.13: Thermal deformations for exhaust existing model at 56.25mm bent radius

Thermal deformations in existing type exhaust manifold is shown in fig 3.12 at 46.875mm and fig 3.13 at 56.25mm bent radius, thermal deformations varies proportionally to the bent radius. Maximum deformations occur at tail pipe. The deformations are more for existing model at 56.25mm bent radius.

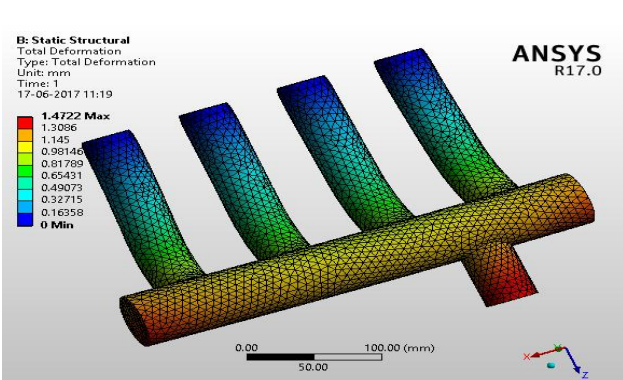


Fig 3.15: Thermal deformations exhaust existing model at 70.3125mm bent radius

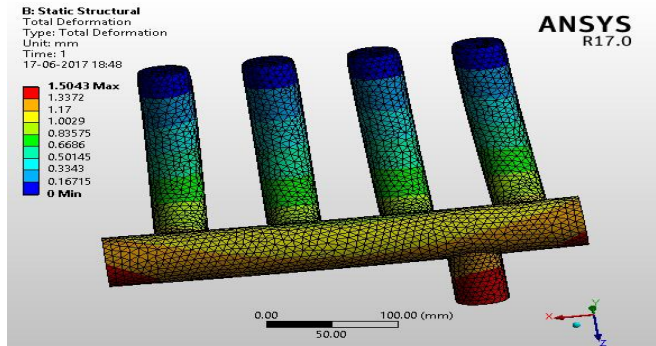


Fig 3.14: Thermal deformations for exhaust existing model at 89.0625mm bent radius

Thermal deformations in existing type exhaust manifold is shown in fig 3.14 at 70.3125mm and fig 3.15 at 89.0625mm bent radius, thermal deformations varies proportionally to the bent radius. Maximum deformations occur at tail pipe. The deformations are more for existing model at 89.0625mm bent radius.

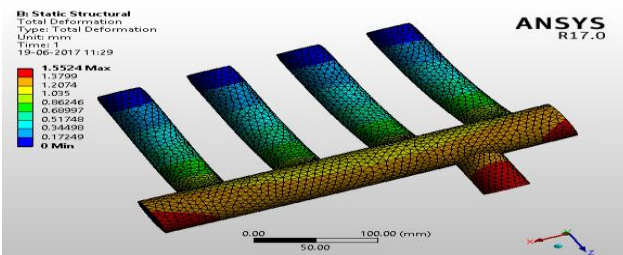


Fig. 3.16: Thermal deformations for exhaust existing model at 112.5mm bent radius

Thermal deformations in existing type exhaust manifold are shown in fig 3.16 at 112.5mm bent radius, thermal deformations varies proportionally to the bent radius. Maximum deformations occur at tail pipe. The deformations are maximum for existing model at 112.5mm bent radius.

3.5 THERMAL DEFORMATIONS IN MODIFIED TYPE EXHAUST MANIFOLD

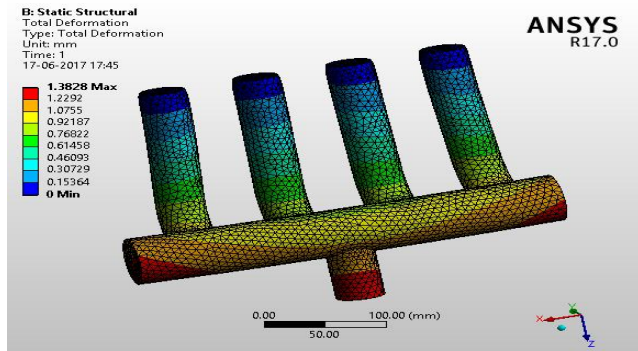


Fig 3.17: Thermal deformations for modified exhaust model at 46.875mm bent radius

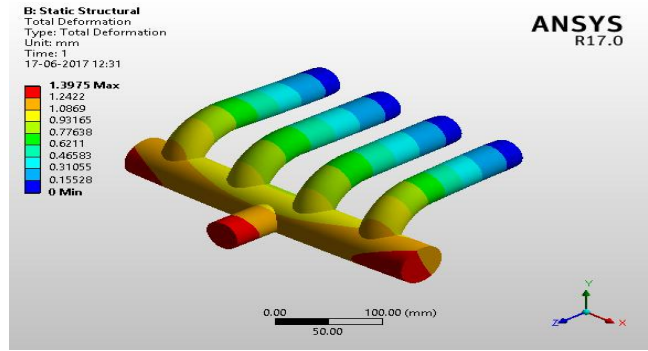


Fig 3.18: Thermal deformations for modified exhaust model at 56.25mm bent radius

Thermal deformations in modified type exhaust manifold is shown in fig 3.17 at 46.875mm and fig 3.18 at 56.25mm bent radius, thermal deformations varies proportionally to the bent radius. Maximum deformations occur at tail pipe. The deformations are less for modified model at 46.875mm and 56.25mm bent radius when compared to existing model of same bent radius.

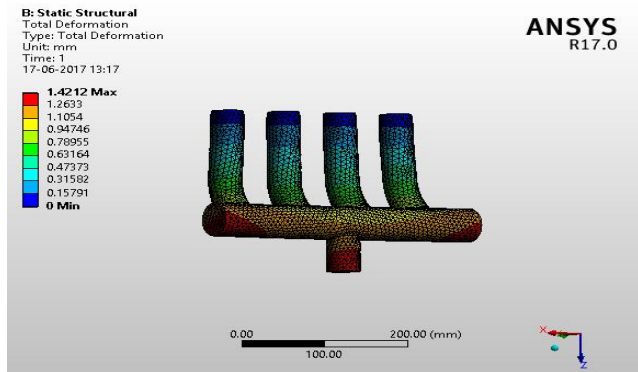


Fig 3.19: Thermal deformations for modified exhaust model at 70.3125mm bent radius

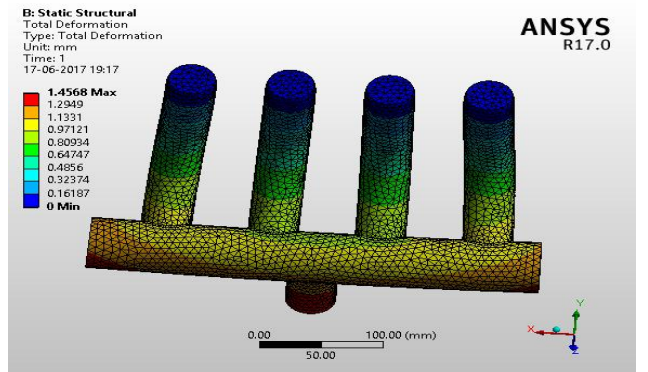


Fig 3.20: Thermal deformations for modified exhaust model at 89.0625mm bent radius

Thermal deformations in modified type exhaust manifold is shown in fig 3.19 at 70.3125mm and fig 3.20 at 89.0625mm bent radius, thermal deformations varies proportionally to the bent radius. Maximum deformations occur at tail pipe. The deformations are less for modified model at 70.3125mm and 89.0625mm bent radius when compared to existing model of same bent radius.

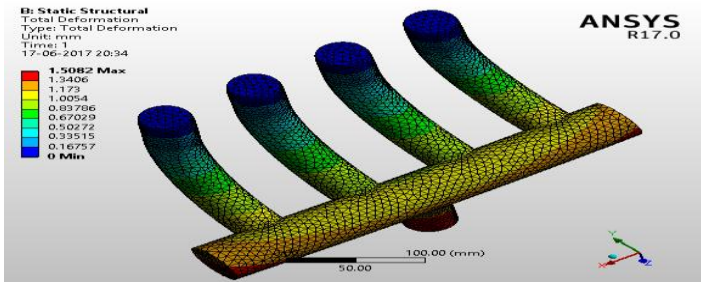


Fig 3.21: Thermal deformations for modified exhaust model at 112.5mm bent radius

Thermal deformations in modified type exhaust manifold is shown in fig 3.21 at 112.5mm and radius, thermal deformations varies proportionally to the bent radius. Maximum deformations occur at tail pipe. The deformations are less for modified model at 112.5mm bent radius when compared to existing model of same bent radius.

3.6 COMPARISON OF THERMAL DEFORMATIONS IN EXISTING AND MODIFIED MODEL

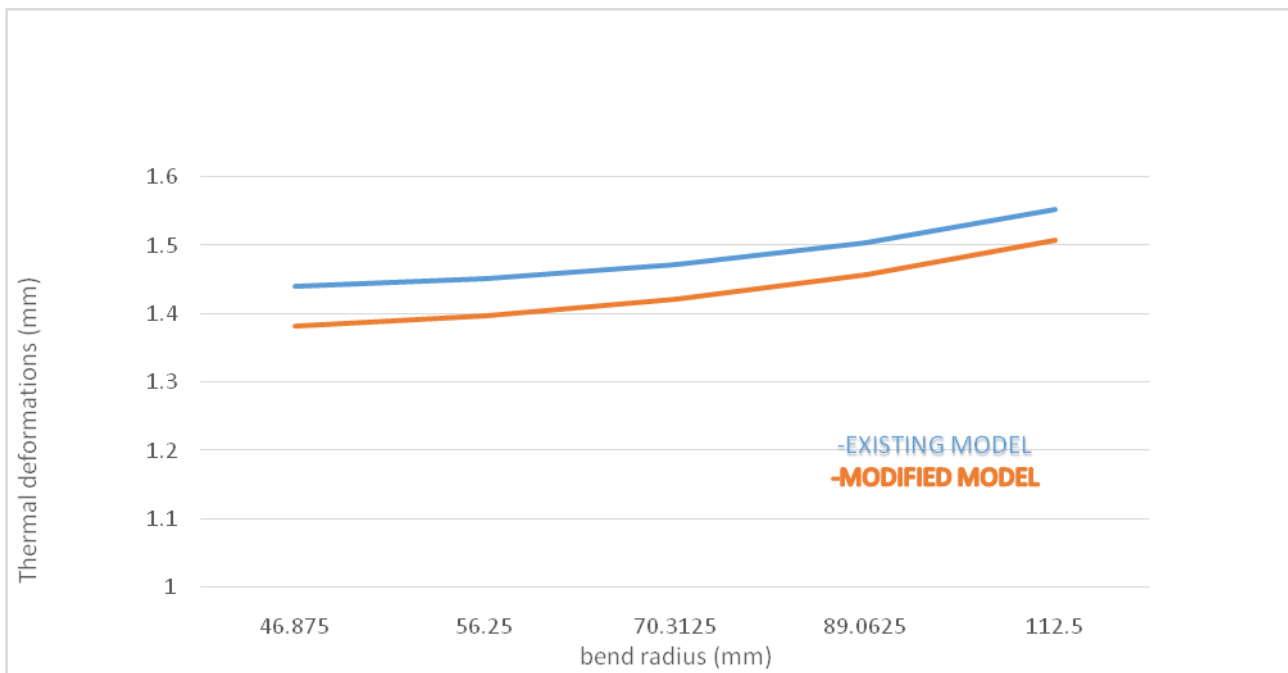


Fig. 3.22: Effect of thermal deformations for exhaust manifold system for both type existing as well as modified type V/S bent radius.

As from the above graphs and figures it is clearly seen that bent radius is proportional thermal deformation. More the bent radius higher will be thermal deformations. The value of thermal deformations are lesser for modified model and more for existing model. So modifying the model is found to be appropriate.

CONCLUSION

1. Existing model shows largest deformation and varies proportionally with the bend radius at the tail pipe where the engine emissions came out. Thermal deformations at 46.875mm bend radius is 1.4404, at 56.25mm bend radius is 1.4518, at 70.3125mm bend radius is 1.4722mm, at 89.0625mm bend radius is 1.5043 and at 112.5mm bend radius is 1.5524mm.
2. Modified model shows lesser deformation and varies proportionally with the bend radius at the tail pipe where the engine emissions came out. Thermal deformations at 46.875mm bend radius is 1.3828, at 56.25mm bend radius is 1.3975, at 70.3125mm bend radius is 1.4212mm, at 89.0625mm bend radius is 1.4568 and at 112.5mm bend radius is 1.5082mm.
3. The difference in pressure drop of two models has been shown in the results. Existing model, the pressure drop is larger and varies inversely to the bend radius and modified model, the pressure drop is lesser when compared with existing model with same bent radius.
4. By the analysis results of thermal deformations and pressure drop, modified model showed less deformations, and less pressure drop than existing model.

FUTURE SCOPE

This design was solely based on taking consideration of pressure drop and thermal deformations issue of exhaust manifold and was found appropriate in terms of manifold designing. But this designing could have been better if it was performed experimentally means setting up a test rig. of exhaust manifold. Involvement of different materials in future for manufacturing of exhaust manifold will help in improved thermal conductivity and better performance.

ACKNOWLEDGEMENT

I take this opportunity to express our sincere thanks to faculty and staff of mechanical engineering Department of **Institute of Engineering & technology**. I would like to thanks the staff members of IC engine lab for sharing the valuable knowledge and experience with us for promoting our work.

REFERENCE

- [1] B Venkata Sai Kiran, Mr. K. Balashankar, "Manifold Optimization of an Internal Combustion Engine by Using CFD Analysis" <http://www.ijmetmr.com/olnovember2015>, ISSN NO:2348-4845.
- [2] A.U Kurbet, S. Dubey, A.R Kumar and S. Razdan, "Design and analysis of exhaust manifold structure subjected to thermo-mechanical loading". IEJR Special issue 2 page 4494-4503,2015, ISSN 2395-1621.
- [3] K. S. Umesh, V. K. Pravin and K. Rajagopal, "Experimental analysis and CFD investigation of multi cylinder four stroke SI engine exhaust manifold for optimal geometry to reduce back pressure and to improve fuel efficiency". International Journal of Automobile Engineering Research and Development (IJAUERD) ISSN(P): 2277-4785; ISSN(E): 2278-9413 Vol. 4, Issue 5, Oct 2014, 13-20.
- [4] Shailda Sharda, R.S Bindu, "Engine exhaust transfer connection design based on high back pressure in exhaust brake applications". IJMPE,ISSN:2320-2092, Volume-2,issue-3,March-2014.
- [5] T. Noguchi, T. Yasuki, T. Nakakubo and T. Atsumi, "Thermal stress and deformations analysis of the exhaust manifold of an internal combustion engine". IJMPE, Volume.2,no-2,1987.

- [6] Miss Pooja Nemade, Dr R.K Patil, "Analysis of exhaust manifold by thermal couple approach". IEJR Special Issue 3 page 375-379, 2016, ISSN 2395-1621.
- [7] Hessamedin Naeimi, Davood Domiry Ganji, Mofid Gorji, Ghasem Javadirad and Moftaba Keshavarj, "A parametric design of compact exhaust manifold junction in heavy duty diesel engine using computational fluid dynamics codes". Year 2011, vol.15, No.4, pp.1023-1033.
- [8] Kyung-Sang Cho, Kyung-Binson, Ue-Kan Kim, "Design of exhaust manifold for pulse converters considering fatigue strength due to vibration". Journal of Korean Society of Marine Engineering, Vol-3, No.7, pp.694-700, 2013 ISSN:1226-9549.
- [9] N.Sabareesh, P.Shiva Raju, M.Achuth Reddy, Srinivas A.S, "Design and analysis of exhaust manifold". IJARSE, Vol. No.6, Issue No.01, Jan 2017.
- [10] Marupilla Akhil Teja, Katari Ayyappa, Sunny Katam, Panga Anusha, "Analysis of exhaust manifold using computational fluid dynamics". Fluid Mech. Open Access 3:129.
- [11] K. Hoschler, J. Bischof, W. Koschel, "Thermo-mechanical analysis of an automotive diesel engine exhaust manifold". Institute for jet propulsion and turbomachinery, RWTH Aachen, D-52062 Aachen.
- [12] Jae Ung Cho, "A study on flow analysis of the exhaust manifold for automobile". IJAER ISSN: 0973-4562, Volume 11, No. 2(2016), pp. 1239-1242.
- [13] Nikhil Kanawade, "Design, analysis and development of 4-cylinder IC engine exhaust manifold". IERJ Page No. 472-478.
- [14] Aakash Sunil Mutkule, Akshay Satpute, Shubham Koshatwar, Saurabh Dharmadhikari, "Thermal and structural analysis of exhaust manifold using FEA approach". IJFEAT ISSN: 2321-8134.
- [15] Xueyuan Zhang, Yu Luo, Jianhua Wang, "Coupled thermos-fluid-solid analysis of engine exhaust manifold considering welding residual stresses". Transactions of JWRI, Special Issue on WSE 2011 (2011).
- [16] Perry, R.H., 1984. "Perry's Chemical Engineers' Handbook", McGraw Hill, New York, 6th edition
Reid, R.C., J.M. Prausnitz and B.E. Poling, 1987. "The Properties of Gases and Liquids", McGrawHill, New York, 4th edition.